Research in Astronomy and Astrophysics, 22:095001 (9pp), 2022 September https://doi.org/10.1088/1674-4527/ac6e5a

Gravitational Deformation Measurement Method for the Main Reflector and Sub-reflector of the 70 m Antenna by Laser Scanner

Lian-Bo Fu[1,2], Jian-Jun Liu[1,2], Wei Yan[1,2], De-Qing Kong[1,2], Xin Ren[1,2], Chen-Di Liu[1,2], and Hong-Bo Zhang[1,2]
[1] Key Laboratory of Lunar and Deep Space Exploration, National Astronomical Observatories, Chinese Academy of Sciences, Beijing 100101, China
fulianbo@bao.ac.cn, liujj@nao.cas.cn, kdq@bao.ac.cn
[2] University of Chinese Academy of Sciences, Beijing 100049, China
Received 2022 February 26; revised 2022 March 28; accepted 2022 April 13; published 2022 August 10

Abstract

Large antennas play an important role in deep space exploration and astronomical research. However, their performances are inevitably affected by the main reflector surface deformation and sub-reflector displacement resulting from the factors of wind, temperature, and gravity, among which the effect of gravity is especially pronounced. In this work, a three-dimensional laser scanner was employed to measure the main reflector and sub-reflector gravitational deformation of the Tianjin 70 m antenna at different elevation angles. Here, we solved the antenna main reflector deformation and sub-reflector displacement, and analyzed the deformation law of the antenna under the action of gravity. A new measurement method of antenna main reflector deformation and sub-reflector displacement is realized by mutual verification of the measured results and theoretical simulations. This method will help to improve the antenna performance and provide a reference to optimize the design of large-aperture antennas.

Key words: telescopes – techniques: radar astronomy – planets and satellites: detection

1. Introduction

Structural deformation will inevitably occur during the operation of large antennas due to wind, temperature, gravity and other factors, seriously affecting the performance parameters. The relative loss of the radiated energy concentration of the antenna panel can be calculated by the gain loss $\Delta G = 685.81\left(\frac{\sigma}{\lambda}\right)^2$ (Qin & Xu 2006), where σ is the standard deviation of the deformation of the main reflector and λ is the wavelength. Currently, the main received signal frequency bands used in deep space exploration are *X* and *Ka* bands. When the antenna works in *X* band, the gain loss is 0.53 dB for 1 mm surface deformation, while the gain loss will reach 6.86 dB for 1 mm surface deformation when using *Ka* band, which leads to serious degradation of antenna performance. In order to meet the requirements of fast adjustment and performance analysis of the large antenna, it is essential to obtain antenna deformation efficiently and with high precision.

Many studies have been conducted on the gravity analysis of large antenna panels. For measuring the deformation of the main reflector, the total station is one of the commonly used methods (Brenner & Britcliffe 2002). However, due to the limitation of a total station instrument, it can only perform the measurement of some angles. Other methods such as holography (Legg et al. 2004) and photogrammetric measurement (Subrahmanyan 2005) were also adopted to obtain the deformation values and the standard deviations of the main reflector at different elevation angles. A three-dimensional laser scanner (3DLS, Christoph et al. 2012, 2017) was adopted to acquire the focal length of the main reflector at different elevation angles. Theoretical simulation was also conducted on the large antenna panels based on finite element analysis to examine the deformation properties under varying conditions of wind, temperature and gravity (Qian et al. 2013).

When the antenna is at different elevation angles, the main reflector deformation and the bracket offset will lead to the displacement of the sub-reflector relative to the ideal position, which will also reduce the antenna's performance. Normally, when a large antenna is built, an *X* band synchronous satellite beacon would scan and obtain the symmetrical directional diagram of the sub-reflector orientation and elevation. This sub-reflector position value is adopted as an initial value of the optimal sub-reflector position. In order to monitor the sub-reflector displacement, the best fitting parabolic method was applied, and based on the ratio of the main reflector and sub-reflector, the amount of adjustment for the sub-reflector can be obtained (Wang et al. 2010). Wang et al. (2014) also adopted a follow-up model and simulated the amount of adjustment for the sub-reflector at different elevation angles, the results of which are consistent with the GRASP simulation results. However, since there are few antennas that can automatically adjust the sub-reflector and many instruments cannot measure the antenna panel data at different elevation angles, research work on the sub-plane is relatively limited.

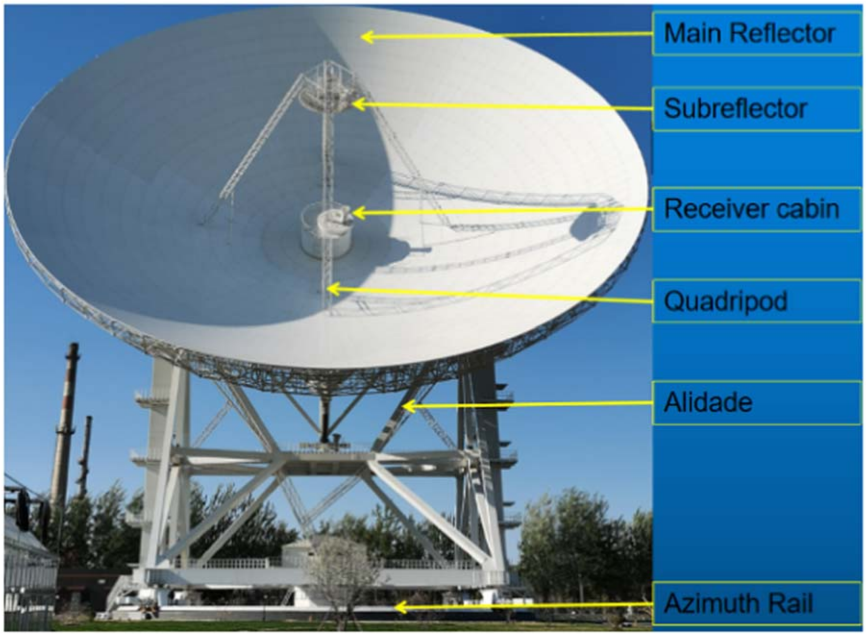

Figure 1. The structure of GRAS-4.

Overall, the analysis of antenna gravity deformation mainly relies on data measurement and theoretical simulation. Data measurement methods include the total station method, photogrammetry measurement, holography, etc., but the results from them are easily affected by factors such as long measurement time and limited observation conditions. As for theoretical analysis, processing errors often occur between the design and the actual processing, and the influence of factors such as wind and temperature under practical conditions may also be underestimated.

To address problems in the study of main reflector deformation and sub-reflector displacement, National Astronomical Observatories, Chinese Academy of Sciences (NAOC) has developed a large antenna deformation detection system. It can acquire a set of antenna data within 90 s and obtain deformation information within 1 hr, with a precision of 1 mm or less. The 3DLS method was employed to realize the analysis of the main reflector deformation and sub-reflector displacement of the antenna. Compared with other methods, the measurement efficiency is greatly improved with guaranteed accuracy, which is necessary for the future real-time adjustment of the antenna.

2. Data Processing Method for Point Cloud Data of Main Reflector and Sub-reflector

In this paper, the main reflector deformation and sub-reflector displacement under the action of gravity were investigated based on the 70 m radio antenna (GRAS-4) at the NAOC Wuqing Station in Tianjin, which has a height of 72 m and a weight of 2700 tons. Its main reflector adopts a modified Cassegrain parabolic surface with a diameter of 70 m, and the area of the antenna is 3840 square meters. GRAS-4 (Figure 1) is the primary data reception antenna of the Tianwen-1 mission.

In order to better analyze the deformation properties of the antenna and verify the correctness of the 3DLS measurement method, theoretical simulation and 3DLS measurement were used together to analyze the gravity effects related to GRAS-4 in this paper.

The GRAS-4 data were collected at 8 p.m. on 2021 August 11 using a 3DLS. The weather on the data acquisition day was clear and cloudy with a wind speed of less than $2\,\mathrm{m\,s^{-1}}$ and temperature of 26° C. We acquired the point cloud data of the antenna at different elevation angles ranging from 10° to 90° with an interval of 10°. The total time for data acquisition lasted for 40 minutes.

2.1. Main Reflector Point Cloud Data Processing Method

For theoretical simulation, the finite element analysis ANSYS Parametric Design Language (APDL) software was used to build the model of GRAS-4, and the model was then imported into finite element analysis. We applied accelerations in different directions to the main reflector to simulate the gravity environment, thus the standard deviations of the main reflector at different elevation angles were obtained.

The actual measurement of GRAS-4 was conducted using 3DLS. The data collection and processing methods are described as follows.

Point cloud data collection. A high precision FARO 3DLS was used to collect main reflector data, which is remotely controlled by a laptop computer. The data collection time is 90 s. The 3DLS emits an active pulse signal, which will be diffusely reflected by the antenna panel and returns to the 3DLS along the same path. In this process, the distance s from the antenna panel to the scanner, and the vertical angle β and horizontal angle α of the pulse signal are recorded, thus information on the antenna panel is quickly obtained

$$P = \begin{bmatrix} X \\ Y \\ Z \end{bmatrix} = \begin{bmatrix} s \cdot \sin\beta \cdot \sin\alpha \\ s \cdot \sin\beta \cdot \cos\alpha \\ s \cdot \cos\beta \end{bmatrix}. \tag{1}$$

Point cloud data filtering. The point cloud data are filtered in three steps. First, the Statistical Outline Remove algorithm (Guo et al. 2019) is applied to statistically filter the discrete point cloud data. Second, the Random Sample Consensus algorithm (Martin & Robert 1980) was employed to exclude data on the sub-reflector and receiver cabin, while diluting the point cloud data. Third, the point cloud data from the main reflector was fitted by higher-order parabolic equations. If the distance of a point cloud datum to the fitted equation is greater than a certain threshold, it was also excluded.

Registration of the main reflector data and acquisition of the deformation variables. Accurate registration between the measured point cloud data and theoretical model was achieved by the parabolic fitting method. The point cloud data coordinates were fitted as parabolic nodes to determine the best-fit paraboloid, which can be expressed in terms of six parameters (Wang et al. 2006): dx, dy, dz, Φ_x, Φ_y and df, where dx, dy, dz are the offsets of the vertices of the best-fit paraboloid with respect to the vertices of the theoretical paraboloid. Φ_x, Φ_y represent the rotation angles of the fitted paraboloid around the original x and y coordinate axes, respectively. df is the relative change of the focal length. The theoretical parabolic equation and the best-fitting parabolic equation can be expressed as

$$z = \frac{x^2 + y^2}{4f}, \tag{2}$$

$$z = \frac{(x - dx)^2 + (y - dy)^2}{4(f + df)} + dz + y \cdot \Phi_x - x \cdot \Phi_y, \tag{3}$$

respectively. According to the approximate inequality

$$\frac{1}{4(f + df)} \approx \frac{1}{4f}\left(1 - \frac{df}{f}\right). \tag{4}$$

The axial error Δz_p between a certain theoretical model point $p(x_p,\ y_p,\ z_p)$ and the corresponding point on the best-fit paraboloid $p'(x_p',\ y_p',\ z_p')$ can be expressed as

$$\Delta z_p = z_p' - \left(z_p - \frac{x_p}{2f}dx - \frac{y_p}{2f}dy + dz + y_p\Phi_x - x_p\Phi_y - \frac{z_p}{f}df\right). \tag{5}$$

Among a total of n sampling points, $(x_s,\ y_s,\ z_s)$ is the coordinate of the sth point and the coordinate of the corresponding offset point is $(x_s',\ y_s',\ z_s')$. In order to achieve registration between the measured point cloud data and the theoretical model, the sum of squares of the axial errors, which is defined as

$$T_w = \sum_{s=1}^{n} \Delta z_s^2, \tag{6}$$

should be the minimized. The condition for T_w to be minimized is that the partial derivatives of the six parameters of the best fitting paraboloid are 0, which are

$$\begin{aligned} &\frac{\partial T_w}{\partial d_x} = 0, \frac{\partial T_w}{\partial d_y} = 0, \frac{\partial T_w}{\partial d_z} = 0, \\ &\frac{\partial T_w}{\partial \Phi_x} = 0, \frac{\partial T_w}{\partial \Phi_y} = 0, \frac{\partial T_w}{\partial d_f} = 0. \end{aligned} \tag{7}$$

The simplification is

$$A_n\beta = H_n, \tag{8}$$

where

$$A_n = \begin{bmatrix} \sum_{s=1}^n \frac{x_s^2}{2f} & \sum_{s=1}^n \frac{x_s y_s}{2f} & -\sum_{s=1}^n x_s & -\sum_{s=1}^n x_s y_s & \sum_{s=1}^n x_s^2 & \sum_{s=1}^n \frac{x_s z_s}{f} \\ \sum_{s=1}^n \frac{x_s y_s}{f} & \sum_{s=1}^n \frac{y_s^2}{2f} & -\sum_{s=1}^n y_s & -\sum_{s=1}^n y_s^2 & \sum_{s=1}^n x_s y_s & \sum_{s=1}^n \frac{y_s z_s}{f} \\ \sum_{s=1}^n \frac{x_s z_s}{f} & \sum_{s=1}^n \frac{y_s z_s}{f} & -\sum_{s=1}^n z_s & -\sum_{s=1}^n y_s z_s & \sum_{s=1}^n x_s z_s & \sum_{s=1}^n \frac{z_s^2}{2f} \\ \sum_{s=1}^n \frac{x_s}{f} & \sum_{s=1}^n \frac{y_s}{f} & -n & -\sum_{s=1}^n y_s & \sum_{s=1}^n x_s & \sum_{s=1}^n \frac{z_s}{f} \end{bmatrix}, \tag{9}$$

$$\beta = \begin{bmatrix} dx & dy & dz & \Phi_x & \Phi_y & df \end{bmatrix}^T, \tag{10}$$

and

$$H_n = \left[\sum_{s=1}^n (z_s - z_s')x_s \ \sum_{s=1}^n (z_s - z_s')y_s \ \times \sum_{s=1}^n (z_s - z_s')z_s \ \sum_{s=1}^n (z_s - z_s')\right]^T. \tag{11}$$

To reduce the error, the weight factor of the sampling point d_i is added, and Equation (8) becomes

$$A_n^T D_n A_n \beta = A_n^T D_n H_n, \tag{12}$$

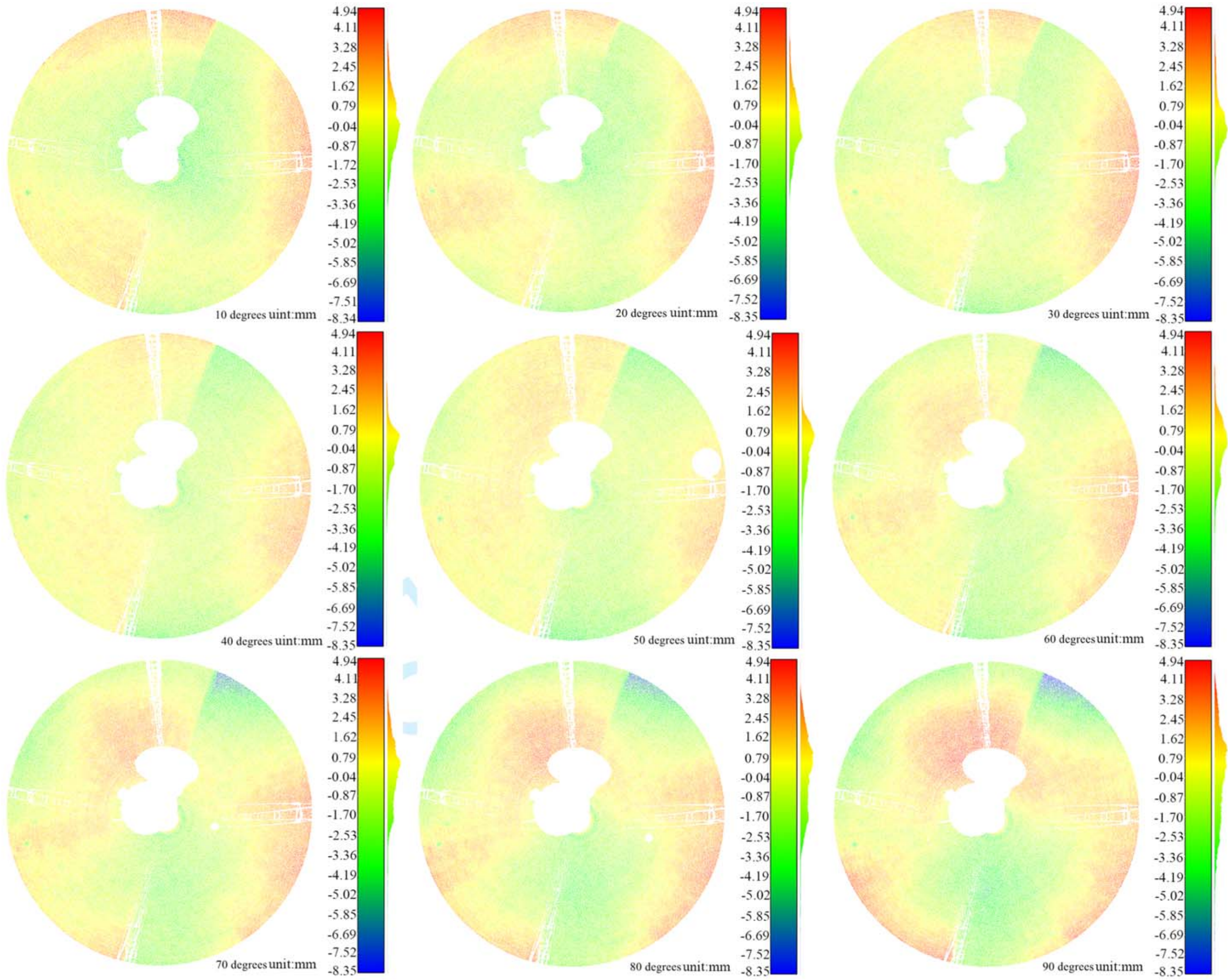

Figure 2. Deformation results of main reflector. (a) 10° deformation result. (b) 20° deformation result. (c) 30° deformation result. (d) 40° deformation result. (e) 50° deformation result. (f) 60° deformation result. (g) 70° deformation result. (h) 80° deformation result. (i) 90° deformation result.

where

$$D_n = \begin{bmatrix} d_1 & 0 & \cdots & 0 \\ 0 & d_2 & \cdots & 0 \\ \cdots & \cdots & \cdots & \cdots \\ 0 & 0 & \cdots & d_i \end{bmatrix}. \tag{13}$$

The weight factor $d_i > 0 (i = 1, 2, \cdots, n)$, and can be expressed as

$$d_i = \frac{n s_i r_i}{\sum_{i=1}^{n} s_i r_i}, \tag{14}$$

where N is the sampling point, s_i is the covering area of the ith sampling point (x_i, y_i, z_i) of the main reflector, $r_i = 1 - (c l_i^2)/R^2$ is the irradiation factor of the corresponding main reflector part where the sampling point is located, C is the ratio of focal length and diameter, R is the antenna aperture, and l_i is the distance between the sampling point and antenna focal axis.

The displacement and rotation matrices are then solved. The accurate registration between the measured point cloud data and theoretical model can be achieved through multiple iterations of rotation and displacement (Zhang 2008). After the registration, information on deformation of the main reflector can be obtained by calculating the distance from the measured main reflector data to the theoretical model. The same process is performed on the point cloud data of the main reflector at other elevation angles to finally obtain information on the deformation.

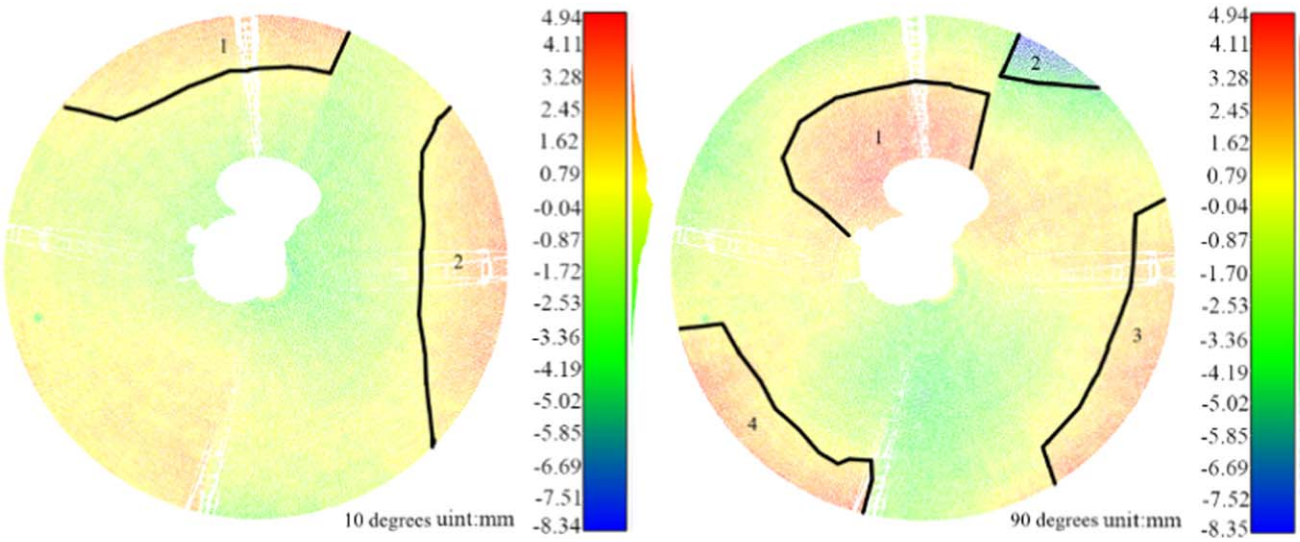

Figure 3. Examples of the main reflector deformation results for large and small elevation angles. (Left) Deformation change of the main reflector at the elevation angle of 10°. Areas 1 and 2 are the main reflector parts with obvious change. Area 1 is at the top of the main reflector with an area of 270 m^2, and Area 2 is at the right side with an area of 340 m^2. (Right) Deformation change of the main reflector at the elevation angle of 90°. The deformation changes are obvious in Areas 1, 2, 3 and 4, which are at the top middle (260 m^2), top right (85 m^2), right (340 m^2) and bottom left (350 m^2) of the main reflector, respectively.

The whole system can complete a set of data acquisition and processing in less than 1 hr, including 1.5 minutes for point cloud data collection, 5 minutes for alignment, 10 minutes for data filtering, 30 minutes for registration and 10 minutes for acquisition of deformation variables.

2.2. Sub-reflector Point Cloud Data Processing Method

The sub-reflector displacement analysis consists of theoretical simulation and 3DLS analysis. Based on the theoretical simulation of the antenna panel model, we obtained the relative displacements of sub-reflector geometric center coordinates at different elevation angles (Guljaina et al. 2020). Sub-reflector displacement includes the amount of rotation in the X direction, the amount of displacement in the Y direction and the amount of displacement in the Z direction. The simulation results are as follows.

Theoretical simulation function of rotation in the X-direction is

$$X = -0.039703 + 0.059365 * \cos(\mathrm{EI}) - 0.000028 * \sin(\mathrm{EI}), \tag{15}$$

theoretical simulation function of translation in the Y direction is

$$Y = 0.037154557 - 0.055563275 * \cos(\mathrm{EI}) + 0.0000352 * \sin(\mathrm{EI}), \tag{16}$$

and theoretical simulation function of translation in the Z direction is

$$Z = 0.005170111 - 0.000114619 * \cos(\mathrm{EI}) - 0.006853667 * \sin(\mathrm{EI}), \tag{17}$$

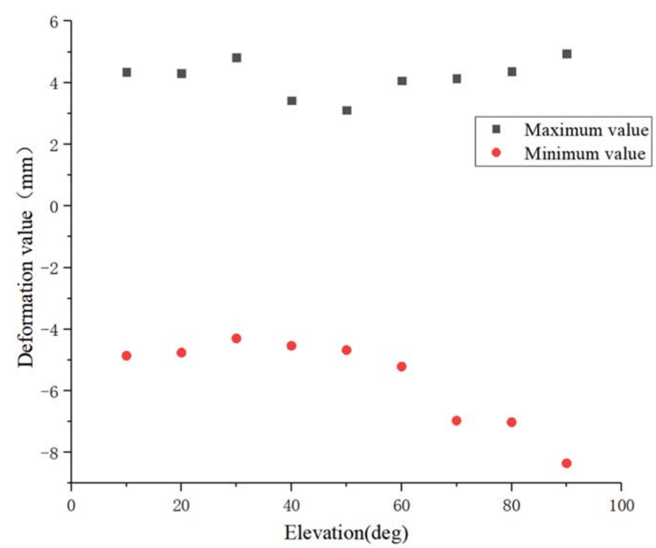

Figure 4. Extreme values of main reflector deformation at different elevation angles.

where EI is the different elevation angles of the antenna. The rotation amounts in the X direction are in radians, while the translation amounts in the Y direction and Z direction are in meters. The R squared of the sub-reflector theoretical simulation displacement equation in all three directions is 0.9999.

The 3DLS acquires the main reflector and also the sub-reflector point cloud data. Several target balls were placed on top of the receiver cabin, and we selected an arbitrary target

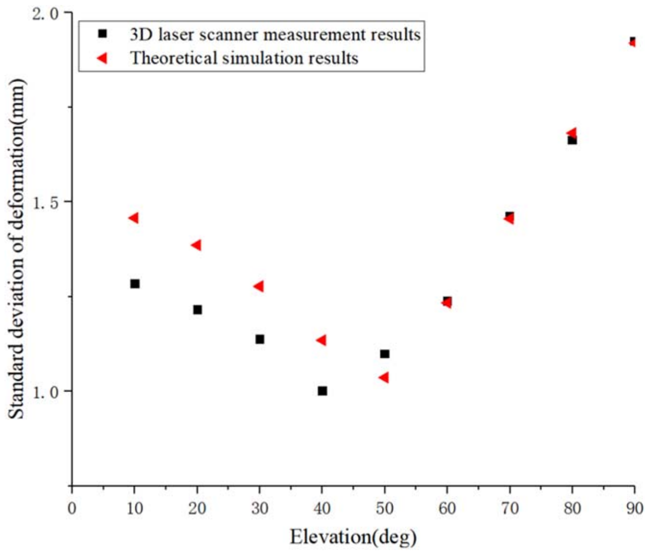

Figure 5. Variation of standard deviation of deformation at different elevation angles. The measured and simulated results are in good agreement. The change in the standard deviations of deformation for small elevation angle is from 0.13 to 0.17 mm, while the change in large elevation angle is from 0.01 to 0.06 mm.

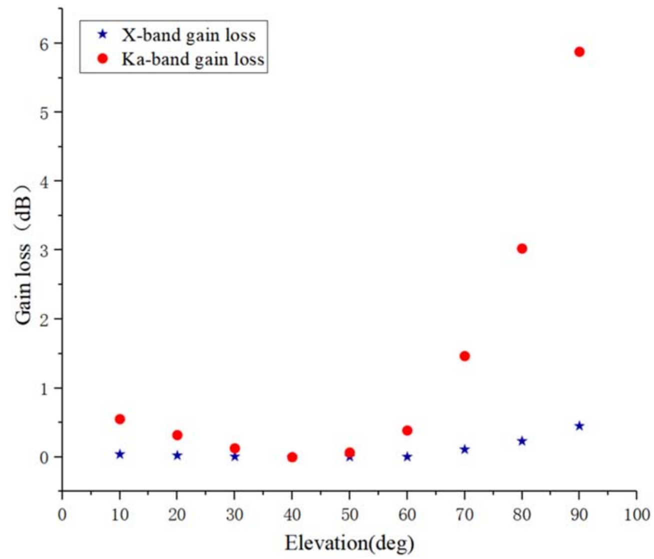

Figure 6. *X* band and *Ka* band gain loss of the main reflector at different elevation angles.

ball and extracted the target spherical coordinate. The distance from the target ball to the geometric center of the sub-reflector was calculated. The displacement and rotation amounts of the sub-reflector in three directions at different elevation angles were acquired. According to the design of the antenna, the best performance of the antenna is at 48°. The difference between the measured results and the simulated results was calculated, and the relationship between the sub-reflector displacement in three directions and elevation angles was fitted and analyzed.

3. Data Processing Results of Main Reflector and Sub-reflector

3.1. Data Processing Results of Main Reflector

The results of the 10°–90° data processing are shown in Figure 2.

Examples of the main reflector deformation results for large and small elevation angles are displayed in Figure 3. We focus on the deformation information on the main reflector at a specific position, extreme value changes of the main reflector and variation of the standard deviation of the main reflector to analyze the deformation laws of the main reflector.

The elevation angles of 10°–40° are considered as the small elevation angles. As depicted in Figure 3 (left), the main reflector parts with obvious change under the condition of small elevation angle are Areas 1 and 2. The deformation of Area 1 changes from 0.82 to 1.66 mm as the elevation angles increase, and the deformation of Area 2 changes from 1.51 to 1.96 mm as the elevation angles increase. For large elevation angle, the main reflector parts with significant deformation are Areas 1, 2, 3 and 4 as marked in Figure 3 (right). The deformation amounts corresponding to Areas 1, 2, 3 and 4 as the elevation angles increase are 1.15 to –3.00 mm, −2.55 to −5.05 mm, 1.06 to 1.72 mm and 0.47 to 1.60 mm, respectively.

The extreme values of main reflector deformation vary regularly with different elevation angles, which can be seen in Figure 4. At the large elevation angles, the maximum deformation values increase from 3.11 to 4.94 mm, and the minimum deformation values increase from −4.68 to −8.35 mm. At the small elevation angles, the maximum deformation values increase from 3.42 to 4.34 mm, and the minimum deformation variation increases from −4.54 to −4.86 mm. The change of extreme values may reflect the main reflector deformation effect under the action of gravity. Though the extreme values are slightly large, they could be due to a measurement error of the 3DLS.

Figure 5 affirms the measured results of the standard deviation of the main reflector are basically consistent with the simulated results, but they are slightly different at small elevation angles. According to the simulation results, the antenna structure with small elevation angles is mainly subjected to transverse force, while the situation with large elevation angles is mainly subjected to longitudinal force. The longitudinal force is better simulated and analyzed than the transverse force, probably resulting in the good consistency between the measured and simulated results for large elevation angles.

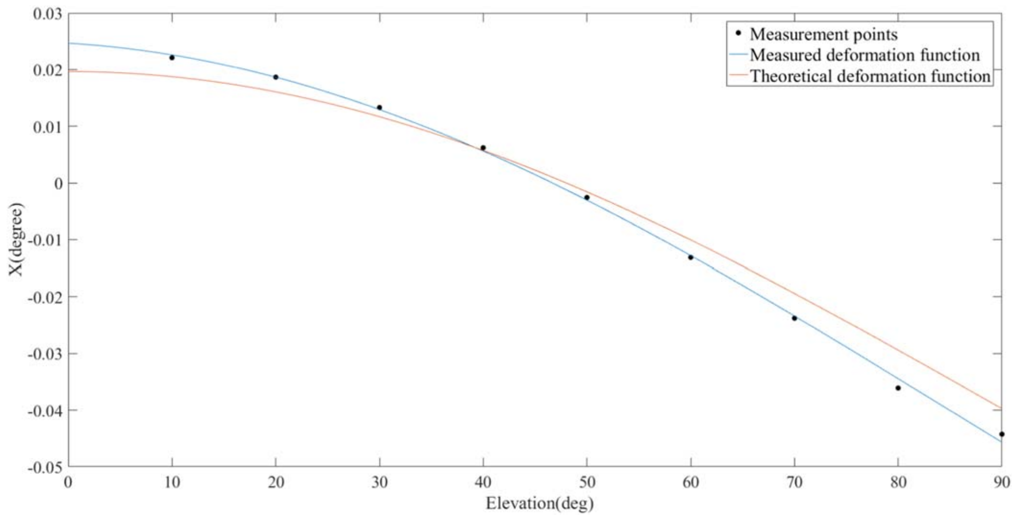

Figure 7. *X* directional displacement of the sub-reflector.

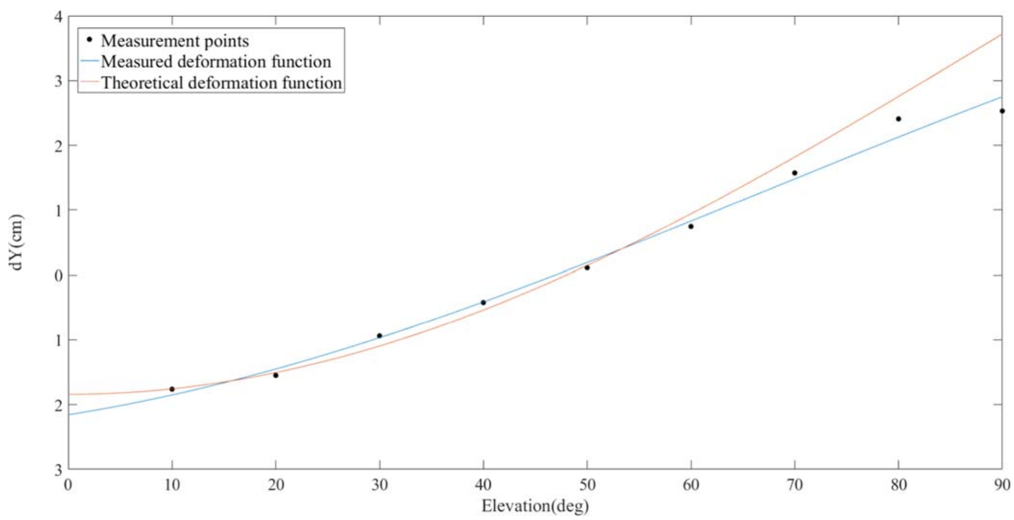

Figure 8. *Y* directional displacement of the sub-reflector.

We also found in Figure 6 that the main reflector deformation may have little effect on antenna performance when using *X* band, while the impact becomes significant when utilizing *Ka* band. In the future, GRAS-4 will apply the *Ka* band in other deep space exploration tasks. It is thus important to measure the deformation of the main reflector at different elevation angles to improve the antenna's performance.

In addition, the good consistency between the measured and simulated results also indicates that 3DLS can achieve accurate measurement and analysis of the main reflector deformation, and this method is more efficient than other methods. Understanding the fast antenna performance is beneficial to optimize the theoretical simulation analysis.

3.2. Sub-surface Data Processing Results

When the main reflector of the antenna is deformed with the change of elevation angles, the sub-reflector will also be displaced. We obtained the amount of rotation for the sub-reflector in the *X* direction, displacement amount in the *Y* direction and the displacement amount in the *Z* direction, which help to improve the concentration of beam received by the main reflector and reduce the gain loss of the antenna. The

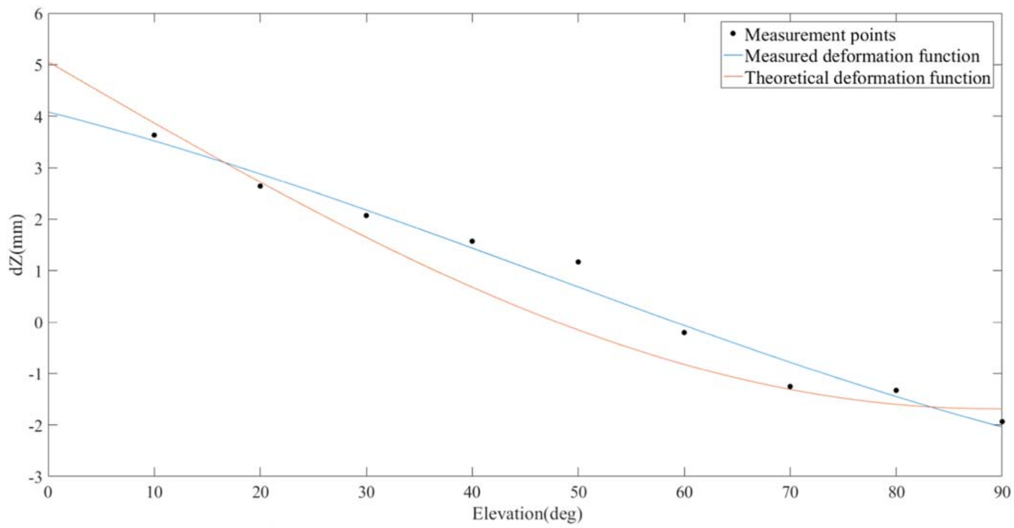

Figure 9. *Z* directional displacement of the sub-reflector.

measured results of the sub-reflector data with different elevation angles are as follows.

In the X direction, the measured fit function is

$$X = -0.03938 + 0.06406 * \cos(\mathrm{EI}) - 0.006293 * \sin(\mathrm{EI}). \tag{18}$$

The comparison of the theoretical simulation and measured results with the change of elevation angle is displayed in Figure 7. The R squared of the sub-reflector measured displacement equation in the x-direction is 0.9987. Within the angles from 10° to 40°, the measured results are larger than the theoretical simulation results. Within 40°–90°, the measured results are smaller than the theoretical analysis results, and as the elevation angles increase, the deviation of the theoretical simulation and measured results becomes larger.

In the Y direction, the measured fit function is

$$Y = 0.01292 - 0.03448\cos(\mathrm{EI}) + 0.01456\sin(\mathrm{EI}). \tag{19}$$

The R squared of the sub-reflector measured displacement equation in the Y direction is 0.9920. As depicted in Figure 8, the theoretical simulation and the measured results are matched relatively well from 10° to 50°. At large elevation angle, the theoretical simulation results are larger than the measured results, and the deviation between them becomes larger with elevation angle increasing.

In the Z direction, the measured fit function is

$$Y = 0.000927 + 0.003154 * \cos(\mathrm{EI}) - 0.002967 * \sin(\mathrm{EI}). \tag{20}$$

It can be seen in Figure 9 that the measured results and the theoretical simulation are in good agreement at 10°, 20°, 70°, 80° and 90°. The R squared of the sub-reflector measured displacement equation in the Z direction is 0.9806. The deviation of the measured results and the theoretical simulation is relatively large at 30°–50°, and the measurement results are larger than the simulation results. However, the measured results and theoretical simulation deviation become smaller at 50°–60°, and also the measurement results are larger than the simulation results.

The Z directional displacement is smaller than the Y directional displacement, which is roughly one order of magnitude different, and the displacement change pattern is a linear regression. The measured and theoretical analysis results of the sub-reflector displacement effect are generally consistent, indicating the measurement method is accurate and credible. The difference between the measured and theoretical analysis results caused by the variation of the antenna structure under the action of gravity is not linear. The 3DLS method realizes displacement measurement of the sub-reflector for the first time, we thus can adjust sub-reflector displacement during the antenna construction and daily maintenance according to the measurement results. Through the displacement results of the sub-reflector measured by this method, the work of the sub-reflector model is carried out, and the antenna efficiency reaches more than 60% over all the elevation angles, which meets the design requirements and engineering tasks of the antenna.

4. Conclusions

In this paper, a new method is implemented to obtain the gravitational deformation effects of the main reflector and sub-reflector of the GRAS-4. The results are compared with the theoretical simulation, which show that the 3DLS method is accurate and reliable. In addition, compared with other methods, the 3D laser scanner has a shorter time to collect data. In the process of measuring data, the influence of the environment on the measurement results can be minimized. The comparison between the measured antenna main surface results and the theoretical simulation results shows that the difference in standard deviation is between 0.01 and 0.17 mm, indicating that the accuracy of the 3D laser scanner reaches the submillimeter level. Through the displacement results of the sub-reflector measured by this method, work on adjusting the sub-reflector model is carried out, and the antenna efficiency reaches more than 60% at the full elevation angle. Though the current measurement error of 3DLS is not ideal, with improvement in the accuracy of 3DLS, it will enrich the antenna deformation measurement method and play a more important role in measuring the antenna deformation.

Overall, the 3DLS method can measure the antenna deformation with high accuracy, high efficiency and high reliability, which has been applied to the Tianwen-1 mission. The 3DLS method successfully realized the measurement and analysis of deformation of GRAS-4 under the action of gravity, which helps to understand and improve the performance of GRAS-4. The 3DLS method provides a reference to optimize the design of a large-aperture antenna in the future.

Acknowledgments

This work was funded by the Key Research Program of the Chinese Academy of Science (ZDBS-SSW-TLC001).

ORCID iDs

Chen-Di Liu https://orcid.org/0000-0002-1767-8219

References

Brenner, M., & Britcliffe, M. J. 2002, IAPM, 44, 187
Christoph, H., David, S., Axel, N., et al. 2017, Senso, 17, 1833
Christoph, H., Philipp, Z., Axel, N., et al. 2012, Journal of Surveying Engineering, 138, 126
Guljaina, k., Xiang, B. B., Wang, N., et al. 2020, AcAAS, 41, 4
Guo, H., Xu, W., Zu, D. H., et al. 2019, Point Cloud Library PCL from Beginner to Master
Legg, T. H., Avery, L. W., Matthews, H. E., et al. 2004, ITAP, 52, 20
Martin, A. F., & Robert, C. B. 1980, Image Understanding Workshop, 71, 78
Qian, H. L., Liu, Y., Fan, F., et al. 2013, International Journal of Space Structures, 28, 15
Qin, S. Y., & Xu, D. 2006, Satellite Communication Earth Station Antenna Engineering Measurement Technology (Beijing: People Post Press)
Subrahmanyan, R. 2005, ITAP, 53, 2590
Wang, C., Duan, B. Y., & Qiu, Y. Y. 2006, Chinese Journal of Radio Science, 21, 403
Wang, J. Q., Yu, L. F., Zhao, R. B., et al. 2014, SSPMA, 44, 1232
Wang, W., Leng, G. J., & Wang, Y. M. 2010, IEEE International Conference on Mechatronics and Automation. IEEE, 2010, 1004
Zhang, K. 2008, Master thesis, Nanjing Normal University School of Geography, Nanjing